1999

Transition state in atomic physics

Charles Jaffé

David Farrelly

T. Uzer

Transition state in atomic physics

Charles Jaffé
Department of Chemistry, West Virginia University, Morgantown, West Virginia 26506-6049

David Farrelly
Department of Chemistry and Biochemistry, Utah State University, Logan, Utah 84322-0300

T. Uzer
School of Physics, Georgia Institute of Technology, Atlanta, Georgia 30332-0430
(Received 30 March 1999)

The transition state is fundamental to modern theories of reaction dynamics: essentially, the transition state is a structure in phase space that all reactive trajectories must cross. While transition-state theory (TST) has been used mainly in chemical physics, it is possible to apply the theory to considerable advantage in any collision problem that involves some form of reaction. Of special interest are systems in which chaotic scattering or half-scattering occurs such as the ionization of Rydberg atoms in external fields. In this paper the ionization dynamics of a hydrogen atom in crossed electric and magnetic fields are shown to possess a transition state: We compute the periodic orbit dividing surface (PODS) which is found *not* to be a dividing surface when projected into configuration space. Although the possibility of a PODS occurring in phase space rather than configuration space has been recognized before, to our knowledge this is the first actual example: its origin is traced directly to the presence of velocity-dependent terms in the Hamiltonian. Our findings establish TST as the method of choice for understanding ionization of Rydberg atoms in the presence of velocity-dependent forces. To demonstrate this TST is used to (i) uncover a multiple-scattering mechanism for ionization and (ii) compute ionization rates. In the process we also develop a method of computing surfaces of section that uses periodic orbits to define the surface, and examine the fractal nature of the dynamics.
[S1050-2947(99)06710-4]

PACS number(s): 32.80.Fb, 45.50.−j, 05.45.−a, 32.60+i

I. INTRODUCTION

The ionization of a hydrogen atom interacting with combinations of external electric and magnetic fields is an intricate problem of fundamental importance [1,2]. In this paper we use modern concepts from chemical physics and nonlinear dynamics to understand this process.

In the past few years innovative, sophisticated experimental techniques have lead to renewed interest in atoms or molecules in which an electron is promoted to a high-energy state, where it is only weakly bound to the core and its dynamics is approximately hydrogenic [3]. These states are typically characterized by very large principal quantum numbers ($n \gtrsim 50$) [4,5], and such atoms (or molecules) are generically known as ''Rydberg'' atoms, because the energy levels of the excited electron are well described by a Rydberg-like formula [4]. More precisely, deviations from the pure hydrogenic eigenenergies are induced by the interaction between the Rydberg electron and the electronic cloud around the atomic or molecular core. These deviations are described by the *quantum defect* δ_l which enters in the formula for the energy levels as a correction to the principal quantum number n [4,6].

Rydberg atoms and molecules occupy a special place in the physical sciences, as their loosely bound electron lives in that poorly charted territory where the quantum world of the atom transforms into the classical reality of macroscopic objects. Rydberg atoms have many exaggerated properties such as huge dipole moments, and they constitute a very convenient, natural laboratory for the investigation of many physical phenomena which they display with exceptional clarity. In these atoms, the Rydberg electron is very weakly bound, and it resides mostly at an immense distance from the atomic or molecular core, to the point that if the Rydberg atoms were solid, they would be just about visible to the naked eye. Laboratory-scale external fields, and even weak stray electric fields [7], become comparable to the atomic, (or molecular) Coulomb field sensed by the Rydberg electron, and interesting dynamical properties, such as, for example, quantum chaology [8–10] can be studied experimentally.

Rydberg atoms in strong external fields constitute fundamental physical systems where the quantum-mechanical regime of strong nonlinearity can be tested [10,11]. While the problem of a Rydberg atom interacting with a strong magnetic field (the quadratic Zeeman effect) has been fairly well understood as a result of sustained research in the past two decades [9,12], the superficially similar scenario resulting from the addition of a perpendicular electric field—the so-called crossed field arrangement [13–18]—remains the least understood of all Rydberg problems. This is all the more regrettable in view of the prominence of the crossed fields in diverse areas of physics ranging from excitonic systems to plasmas and neutron stars. This problem is so complex because no continuous symmetry survives the extensive symmetry breaking [19] induced by the two fields. The result is a wealth of new physics which is only possible beyond two degrees of freedom, such as Arnol'd diffusion [10,20,21]. This absence of symmetry also allows localizing electronic

wave packets in all spatial dimensions, and the observation of these localized wave packets [22] has led to new insights into the dynamics of the electron in the correspondence principle regime. It has also been found that a velocity-dependent, Coriolis-like force in Newton's equations causes the ionization of the electron to exhibit chaotic scattering [23,24]. All these phenomena, as well as renewed interest in the motional Stark effect [25,26], make the crossed-field problem an experimentally accessible paradigm for a wide variety of outstanding issues in atomic and molecular physics, solid-state physics [27,28], nuclear physics [29], astrophysics [30], and celestial mechanics [31].

The experimental challenge has been taken up by Raithel, Fauth, and Walther [16,32] who in a landmark of experiments have identified a class of quasi-Landau (QL) resonances in the spectra of rubidium Rydberg atoms in crossed electric and magnetic fields. Similar to the original QL resonances observed by Garton and Tomkins [33], this set of resonances is associated with a rather small set of *planar* orbits of the crossed-field Hamiltonian which is known to support an enormous number of mostly nonplanar periodic motions [16].

More recent experiments [34] showed that the ionization threshold has a nontrivial progression with respect to the external fields. Its classical-like scaling behavior (i.e., the progression was found to depend on the scaled fields alone) [34] suggested the possibility of a classical explanation. Recently, two of us documented this classical mechanism [24] which explains and consolidates these findings for energies below, at, and above threshold by showing that the atom undergoes its transition to chaotic scattering due to the existence of a critical point in the Hamiltonian flow.

The problem of ionization of a Rydberg atom in crossed magnetic and electric fields resembles a chemical reaction: in a typical unimolecular reaction [35] the molecule is first ''activated'' by the injection of sufficient energy, so that it can overcome the barrier to reaction. Some time after the activation, if energy finds its way into the reactive mode, the reaction occurs. In the problem of the ionization of Rydberg atoms the ''activation'' is the initial excitation to a state of very high principal quantum number ($n \sim 50$ or larger). Following state preparation, energy flows into the ionization channel and the electron is detached. In both systems a central question concerns the rate at which the energy migrates into the reactive (or ionizing) mode. In this paper we develop an approach to the ionization of Rydberg atoms in crossed electric and magnetic fields that builds on recent advances in the theory of chemical reaction dynamics [36,37]. The key to describing a chemical reaction is the recognition of the importance of classical phase-space structures (bottlenecks, turnstiles, etc.) that govern the progress of the reaction [38]. Identifying these structures requires techniques from nonlinear dynamics and chaotic scattering theory. We apply and extend these methods to treat the ionization of Rydberg atoms in crossed electric and magnetic fields, and we find that this intricate process can be described in this manner. Let us begin with a review of transition-state theory and requisite nonlinear dynamics.

The concept of a transition state is central to the theory of chemical reaction dynamics [39]. Its role in atomic physics has been discussed by Fano [66]; also see Ref. [67]. The basic idea, which is strictly classical in origin, is that there exists a minimal set of states that all reactive trajectories must pass through and which is never encountered by any nonreactive trajectories. This set of states is collectively called the ''transition state.'' We will demonstrate that this model not only holds for the ionization of a hydrogen atom in crossed magnetic and electric fields, but that it provides probably the only way to picture the mechanism of ionization. We choose this system because it encapsulates all of the key ingredients of transition-state theory (TST), and it raises a number of issues that are not normally encountered when applying transition-state theory to chemical reactions: the most significant feature we discover is a periodic orbit dividing surface (PODS) (more on these below) that exists in phase space rather than in configuration space, as has been exclusively the case up until now. This novelty can be traced directly to the presence of velocity-dependent forces that result from the symmetry breaking due to the crossed fields configuration. Velocity-dependent forces have confounded many previous attempts to describe the ionization dynamics of this problem [34] and account for the large number of experimental and theoretical studies of this system. So far, no general consensus has emerged as to the mechanism of ionization. Here we show that TST provides a direct approach to describing and understanding the ionization dynamics in this large class of experimentally important problems.

The notion of a transition state can be traced to the work of Marcelin [40] in 1915. Subsequently, in 1931, Eyring and Polanyi [41] quantified the idea of a transition state in the collinear $H+H_2$ reaction. Their paper, which must be viewed as the origin of modern theories of chemical reactions, reports the first calculation of the potential-energy surface of a reaction. This surface consists of two valleys, one associated with the reactants and the other with the products, separated by a potential barrier (the small minimum that was thought to lie at the top of the potential barrier, ''Lake Eyring,'' was subsequently shown to be an artifact [42]). Using this surface, Eyring and Polanyi defined the transition state as the path of steepest ascent from the saddle point of the barrier. After the system has surmounted the barrier and crossed the transition state, the forces are such that they push the system even farther out into the products valley. Thus it would appear that the system can never recross the transition state to return to the reactants side of the potential; in other words, that the transition state is a surface of no return. This analysis is flawed, as will be discussed shortly.

Immediately following the appearance of this work, Wigner [43] and others [44,45], developed a variety of very simple, yet extremely useful, theories of bimolecular reactions, for example, activated complex theory and transition-state theory. During the next decade further seminal papers in the development of unimolecular reactions were published [35]. Again the concept of a transition state played a central role, although these early theories of chemical reactions remained strictly classical in nature. Quantization was the next major step in the development of transition-state theory [47].

Even in the earliest days it was recognized that the transition state, as defined by Eyring and Polanyi, was in fact not a surface of no return, and that trajectories can recross this surface many times [48]. This is due to the existence of

dynamical effects that can result from cross-terms in the kinetic energy, for example dynamical barriers [49]. The recognition of the complex nature of the dynamics led to the development of a variational approach [45–47]. Here the central idea is to consider the set of all possible transition states and then to choose the one with the minimum flux across it. Clearly, if trajectories recross a prospective transition state, then these trajectories will be counted more than once in the computation of the flux. Pechukas [50] solved the variational problem by demonstrating that the surface of minimum flux, and hence the transition state, must be an unstable periodic orbit whose projection into coordinate space connects the two branches of the relevant equipotentials. These surfaces are called ''periodic orbit dividing surfaces'' or PODS (as is the convention, we decree that the term PODS be both singular and plural [51]). The PODS with the minimum flux is chosen as the transition state.

While the original idea of a transition state was expressed as a dividing surface in *coordinate* space, it was soon recognized that a proper treatment must be in terms of dividing surfaces in *phase space*. From this point of view the goal is to partition phase space into volumes corresponding to reactants and products. Progress in this direction had to wait for two developments: (i) advances in the study of dynamical systems, and (ii) access to sufficiently powerful computers. In the mid 1980s Davis and co-workers [36] studied the phase space dynamics of a number of reactive systems. They have shown that the partitioning of phase space can be accomplished using the manifolds of the PODS associated with the transition states. Another related approach to the investigation of the structure of phase space of reactive systems, which is closer to the approach adapted here, is that of Ozorio de Almeida *et al.* [37]. Tiyapan and Jaffé [52] extended these ideas considerably, and showed that the manifolds of the PODS can be used to construct an invariant fractal tiling of phase space, and in the simplest case of complex formation (unimolecular reactions) have characterized this fractal structure.

This paper is organized as follows: Section II introduces the Hamiltonian for the hydrogen atom in crossed fields which we treat in the planar limit. This approximation is expected to capture most of the essential dynamics, because the planar model has proved extremely useful in explaining experimental observations [34]. The transition state itself is introduced in Sec. III, which identifies an unusual class of PODS that ionizing trajectories must pass. The treatment of the half-scattering problem is contrasted to that needed for a full collision in Sec. IV. Conclusions are in Sec. V.

II. PLANAR CROSSED-FIELD PROBLEM

In the present work we are interested in a particular aspect of this problem: chaotic ionization in the sense that residence times of the electron inside the Stark saddle point show a fractal structure [53]. This ionization can be thought of as chaotic half-scattering, since there is no flux of incoming electrons and the system starts out in a quasibound state, as opposed to the conventional case of chaotic scattering in which the system is unbound in both asymptotes. Chaotic scattering leads to observable fractal signatures in the quantum mechanics. Indeed, the best-known indicator of chaotic scattering systems, namely, Ericsson fluctuations, has been detected numerically in this system by Main and Wunner [23] who showed that, above the threshold, the electron dynamics is scattering and chaotic.

As an additional twist, a potential-energy surface cannot be defined for this system because a nonconserved paramagnetic term mixes coordinates and momenta [see Eq. (8) below]. Consequently, the equations of motion are not symmetric with respect to time reversal, and the traditional analysis of transition-state theory employing a potential-energy surface must be generalized.

At this point it is useful to introduce the concept of a surface of zero relative velocity to understand the motion of the electron in a rotating frame which is the most convenient frame for studying the dynamics. A consequence of Newton's second law is that if a conservative force $\mathbf{P}=-\boldsymbol{\nabla}V$ acts on a particle, then motion with respect to axes that are rotating with constant angular velocity ω about the z axis will be determined by

$$P=m[\ddot{\mathbf{r}}+\{2\omega\hat{\mathbf{z}}\times\dot{\mathbf{r}}\}+\{\omega^2\hat{\mathbf{z}}\times(\hat{\mathbf{z}}\times\mathbf{r})\}], \tag{1}$$

where the extra terms as compared to Newton's second law in an inertial frame in the first and second sets of curly braces are the Coriolis and centrifugal forces, respectively. The following relation has also been used

$$\frac{d\mathbf{r}}{dt}=\frac{\partial\mathbf{r}}{\partial t}+\omega\times\mathbf{r}, \tag{2}$$

which relates the (total) rate of change of a vector $\mathbf{r}$ in a fixed frame of reference to that in a frame rotating with angular velocity ω. If $\mathbf{r}$ is decomposed into perpendicular and planar components as

$$\mathbf{r}=z\hat{\mathbf{z}}+\rho, \tag{3}$$

then

$$\mathbf{P}=m[\ddot{\mathbf{r}}+2\omega\hat{\mathbf{z}}\times\dot{\mathbf{r}}+\omega^2\boldsymbol{\rho}]. \tag{4}$$

Using the relation $\rho\cdot\dot{r}=\boldsymbol{\rho}\cdot\dot{\boldsymbol{\rho}}$ and forming the quantity $\mathbf{P}\cdot\dot{\mathbf{r}}$, we can calculate the work done in going from A to B:

$$W_{AB}=\int_A^B\mathbf{P}\cdot d\mathbf{r}=\frac{m}{2}(v_B^2-v_A^2)-\frac{m\omega^2}{2}(\rho_B^2-\rho_A^2), \tag{5}$$

where v_A and v_B are the mechanical velocities. For a conservative field $W_{AB}=V(A)-V(B)$, and so we obtain the result

$$\tfrac{1}{2}m\dot{\mathbf{r}}^2+V-\tfrac{1}{2}m\omega^2\rho^2=\text{const}. \tag{6}$$

It is apparent that the motion in the rotating frame is governed by the *modified* potential energy function

$$\Omega(x,y,z)=V-\tfrac{1}{2}m\omega^2\rho^2, \tag{7}$$

which for fixed Ω is the locus of the surfaces of zero velocity. In celestial mechanics the surface defined by $\Omega(x,y,z)$ is often called the *surface of zero relative velocity* or simply the *zero-velocity surface* [54,55].

A. Hamiltonian

The Hamiltonian (in atomic units) for the planar hydrogen atom in crossed electric and magnetic fields in Cartesian coordinates is

$$H=\frac{1}{2}(P_X^2+P_Y^2)-\frac{1}{R}+\left[\frac{\omega_c}{2}(XP_Y-YP_X)+\frac{\omega_c^2}{8}(X^2+Y^2)-\mathcal{E}X\right], \tag{8}$$

where $R=\sqrt{X^2+Y^2}$, ω_c is the cyclotron frequency, and $\mathcal{E}$ is the electric field. The three terms in the brackets are due to the external fields: the first is the paramagnetic term, the second is the diamagnetic term, and the third is the electric-field interaction. The paramagnetic term gives rise to the velocity-dependent forces. Defining scaled coordinates Q and time T,

$$Q=\omega_c^{2/3}q, \qquad T=\omega_c^{-1}t, \tag{9}$$

the Hamiltonian becomes

$$\mathcal{H}=\frac{1}{2}(P_x^2+P_y^2)-\frac{1}{r}+\left[\frac{1}{2}(xP_y-yP_x)+\frac{1}{8}(x^2+y^2)-\varepsilon x\right]. \tag{10}$$

Here $\mathcal{H}=\omega_c^{-2/3}H$ is the scaled energy, $\varepsilon=\omega_c^{-4/3}\mathcal{E}$ is the scaled electric-field strength, and $r=\sqrt{x^2+y^2}$. This Hamiltonian has a single critical point that is usually called the Stark saddle point.

The Coulombic singularity results in significant numerical difficulties which can be minimized by the method of *classical regularization* [56]. This is accomplished by first transforming to semiparabolic coordinates,

$$x=\frac{1}{2}(U^2-V^2)\quad P_x=\frac{UP_U-VP_V}{U^2+V^2}, \qquad y=UV\quad P_y=\frac{VP_U+UP_V}{U^2+V^2}, \tag{11}$$

which yields

$$\mathcal{H}=\frac{1}{2}\frac{P_U^2+P_V^2}{U^2+V^2}-\frac{2}{U^2+V^2}+\frac{1}{4}(UP_V-VP_U)+\frac{1}{32}(U^2+V^2)^2-\frac{\varepsilon}{2}(U^2-V^2). \tag{12}$$

We now define a new Hamiltonian by multiplying by (U^2+V^2) and rearranging terms; this yields

$$\mathcal{K}=2=\frac{1}{2}(P_U^2+P_V^2)-\mathcal{H}(U^2+V^2)+\frac{1}{4}(U^2+V^2)(UP_V-VP_U)+\frac{1}{32}(U^2+V^2)^3-\frac{\varepsilon}{2}(U^4-V^4). \tag{13}$$

Having defined a new Hamiltonian, we have also redefined the time variable. The regularized time is given by

$$\frac{d\tau}{dt}=(U^2+V^2)^{-1}. \tag{14}$$

When the scaled energy is negative ($\mathcal{H}<0$) the regularized Hamiltonian given in Eq. (13) is that of two coupled isotropic harmonic oscillators with frequency $\Omega=\sqrt{-2\mathcal{H}}$. In order to place this Hamiltonian into a more standard form, we scale the coordinates and time once more:

$$Q=\Omega^{-1/2}q, \qquad T=\Omega^{-1}t. \tag{15}$$

This yields

$$K=\frac{2}{\Omega}=\frac{1}{2}(P_u^2+P_v^2)+\frac{1}{2}(u^2+v^2)+\frac{1}{4\Omega^2}(u^2+v^2)(uP_v-vP_u)+\frac{1}{32\Omega^4}(u^2+v^2)^3-\frac{\varepsilon}{2\Omega^3}(u^4-v^4). \tag{16}$$

The equations of motion are given by

$$\begin{aligned}
\dot{u}&=P_u-\frac{1}{4\Omega^2}v(u^2+v^2),\\
\dot{v}&=P_v+\frac{1}{4\Omega^2}u(u^2+v^2),\\
\dot{P}_u&=-u+\frac{2\varepsilon}{\Omega^3}u^3-\frac{1}{2\Omega^2}u(uP_v-vP_u)-\frac{1}{4\Omega^2}P_v(u^2+v^2)-\frac{3}{16\Omega^4}u(u^2+v^2)^2.\\
\dot{P}_v&=-v-\frac{2\varepsilon}{\Omega^3}v^3-\frac{1}{2\Omega^2}v(uP_v-vP_u)+\frac{1}{4\Omega^2}P_u(u^2+v^2)-\frac{3}{16\Omega^4}v(u^2+v^2)^2.
\end{aligned} \tag{17}$$

Recall that under time-reversal the dynamical variables transform as

$$Q\to Q,\quad \dot{Q}\to-\dot{Q}, \qquad P\to-P,\quad \dot{P}\to\dot{P}, \tag{18}$$

and therefore these equations are not symmetric with respect to time reversal. In addition, care must be taken in interpreting results obtained from these equations because regularization doubles the volume of phase space. This is readily seen by inverting the transformation equations, Eq. (11).

B. Dynamics

The dynamics of the planar crossed-field problem have been investigated [24] as a function of the scaled electric-field strength for a single value of the scaled energy, $\mathcal{H}=$

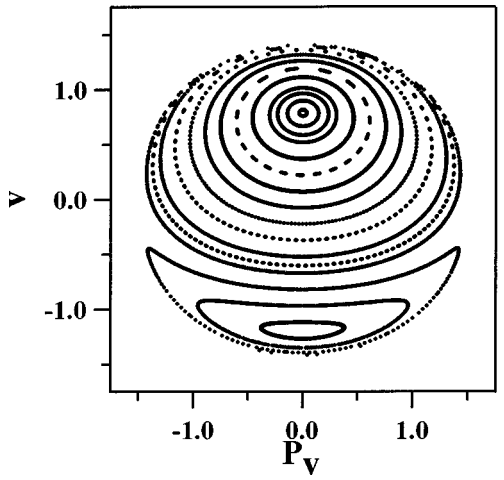

FIG. 1. Shown here is the $(v\text{-}P_v)$ surface of section $(u=0,\dot{u}\geqslant 0)$ for an electric-field strength of $\varepsilon=0.4$. This is well below the onset of chaotic behavior. The two principal periodic orbits of the system lie at the center of the two sets nested of *KAM* curves. These are shown in Fig. 2. The sets of nested *KAM* curves are not separated by a separatrix; this will be discussed subsequently. The upper periodic orbit corresponds to the upfield case and the lower periodic orbit corresponds to the downfield case. The axes are the scaled coordinate and momentum.

-1.52. The planar system is, of course, integrable for $\varepsilon=0$. We observe the onset of chaos at approximately $\varepsilon_{\rm crit}\sim 0.5757$, which is below the ionization threshold for this value of the energy, that is, $\varepsilon=\mathcal{H}^2/4=0.5776$.

Before proceeding to identify the transition state, we first give a brief overview of the structure of phase space as one traverses $\varepsilon_{\rm crit}$. Figure 1 shows the $(v\text{-}P_v)$ surface of section $(u=0.\dot{u}\geqslant 0)$ for $\varepsilon=0.4$ which is well before the onset of chaos. The two periodic orbits that lie at the center of the two sets of nested Kolmogorov, Armol'd, and Moser (KAM) curves [20] are shown in Fig. 2 in both regularized and Cartesian coordinates. We use these two orbits to define the fundamental dynamical modes of the system. The central periodic orbit in the lower set of nested *KAM* curves is the ''downfield'' periodic orbit which we label (ii), and that in the upper set of nested *KAM* curves is the ''upfield'' periodic orbit which we label (i). These two periodic orbits exist throughout the range of ε investigated.

Figure 3 shows the surface of section for a field strength of $\varepsilon=0.5765$ which is above the onset of chaos but still below the ionization threshold. The full surface of section is shown in Fig. 3(a), while an enlargement of the chaotic region is provided in Fig. 3(b). First observe that the volume of the chaotic region is quite small and is not readily seen in Fig. 3(a). Figure 3(b) reveals that the chaotic trajectories lie in an annulus surrounding the periodic orbit (ii). Figure 4 shows the chaotic region of phase space at the ionization threshold, $\varepsilon=0.5776$. Again we see that in the center of the chaotic sea there is an island of stability centered on the periodic orbit (ii). In phase space, for values of ε below the ionization threshold $(\varepsilon<0.5776)$, the energy shell on which the dynamics is confined consist of two separate parts corresponding to the bound and scattering dynamics. At the ionization threshold these two parts come into contact precisely at the Stark saddle.

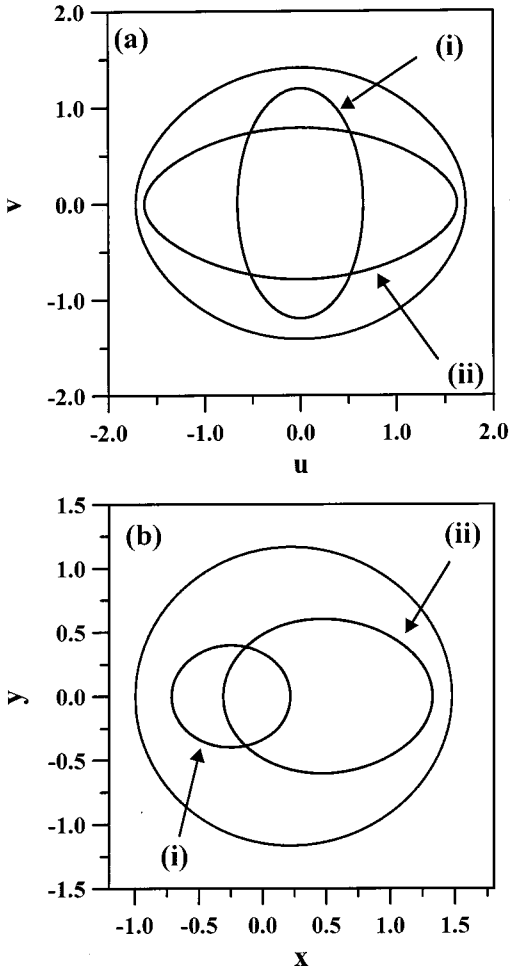

FIG. 2. Shown here are the two principal periodic orbits for an electric-field strength of $\varepsilon=0.4$. In (a) they are shown in the regularized coordinates (u, v), and in (b) they are shown in the Cartesian coordinates (x,y). The orbit labeled (i) corresponds to the central periodic orbit (upfield) of the lower set of nested *KAM* curves in Fig. 1, while the orbit labeled (ii) is the central periodic orbit (downfield) of the upper set of nested *KAM* curves. The axes are scale coordinates.

Surfaces of section for three values of the electric field strength $(\varepsilon=0.5785,\ 0.58,\ \text{and}\ 0.6)$ which all lie above the ionization threshold are shown in Fig. 5. First observe that the two parts of the energy shell come together in such a manner as to drain the chaotic sea through ionization. Also note that the periodic orbit (ii) remains stable for a considerable range above the threshold. At $\varepsilon=0.6$ [Fig. 5(c)] this orbit has, at last, become unstable, and the central island of stability has disappeared. Nevertheless, evidence of island chains of stability is observed.

The central question to be discussed shortly concerns the existence of a transition state lying above the Stark saddle. We will demonstrate its existence by construction, and then use it to investigate the dynamics of ionization.

III. TRANSITION STATE

In Hamiltonian systems for which there is a clearly defined potential energy, the problem of finding the transition state is straightforward: one searches for a periodic orbit whose projection into coordinate space begins and ends at

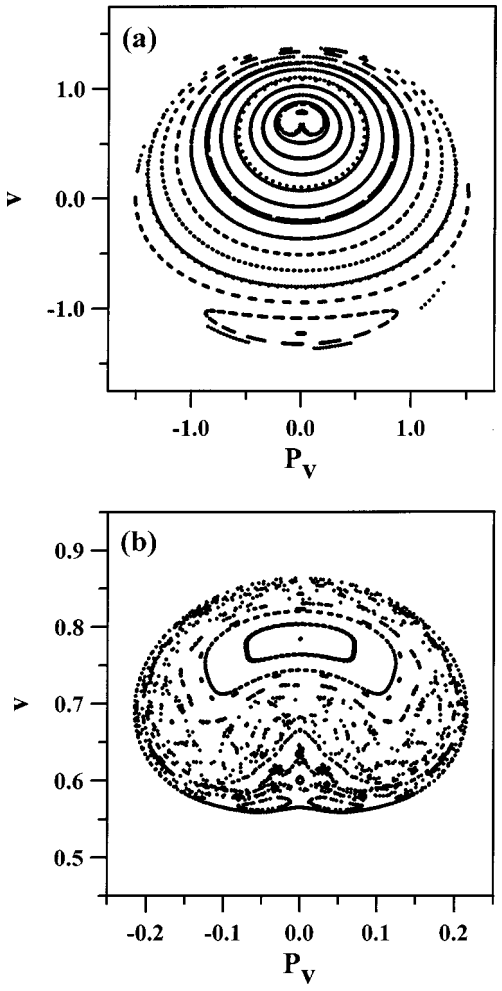

FIG. 3. Shown here is the $(v\text{-}P_v)$ surface of section $(u=0,\dot{u}\geqslant 0)$ for an electric-field strength of $\varepsilon=0.5765$. This is just above the onset of chaotic behavior. The full surface of section is shown in (a), and an enlargement of the region surrounding the central periodic orbit of the upper set of nested *KAM* curves is shown in (b). Comparison of these two figures shows that the chaotic trajectories fill a very small region of phase space and that the central periodic orbit (*ii*) remains stable and is surrounded by *KAM* curves which form an island in the chaotic sea. The axes are the scaled coordinate and the momentum.

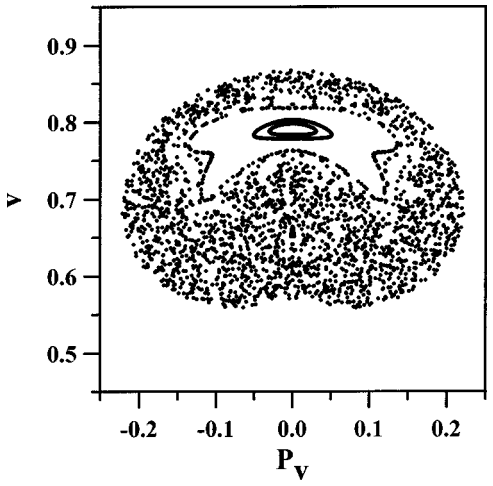

FIG. 4. Shown here is an enlargement of the chaotic region in the $(v\text{-}P_v)$ surface of section $(u=0,\dot{u}\geqslant 0)$ for an electric-field strength of $\varepsilon=0.5776$. This is well above the onset of chaotic behavior, and corresponds to the ionization threshold. Observe that the central periodic orbit (*ii*) is stable and surrounded by *KAM* curves forming an island in the chaotic sea. The axes are the scaled coordinate and the momentum.

the classical boundaries (see Fig. 6). In coordinate space the classical boundaries are given by the equipotentials, and, for a system with two degrees of freedom, the position on an equipotential can be specified by a single parameter. Thus, numerically, the procedure involves a simple one-parameter search. One approach is to construct a convenient surface of section using the locus of points defining the equipotential as initial conditions. One considers the first and second intersections of the equipotential in the surface of section. We refer to these intersections as the first and second images of the equipotentials. The intersections of these two images correspond to periodic orbits. In this manner one finds two different types of periodic orbits. The first type touches both branches of the equipotential and intersect the surface of section at a single point (and thus is period 1). The second type touches one of the branches of the equipotential twice at different points. These orbits intersect the surface of section at two different points, and thus are period-2 orbits. The periodic orbit for which one is searching is of the first type. This is illustrated in Fig. 6.

Unfortunately, this approach is not immediately applicable when one cannot define a potential-energy surface as in the problem at hand. The technical obstacle to progress is that the equations of motion are not symmetric with respect to time reversal. To make this clear, consider a trajectory whose projection into coordinate space touches the classical boundary. If the equations of motion were symmetric with respect to time reversal, then, a trajectory which leaves the classical boundary would retrace, in coordinate space, its approach to the classical boundary. In other words, the time development of the variables would satisfy

$$q(-t+t_0)=q(t+t_0),$$
$$\dot{q}(-t+t_0)=-\dot{q}(t+t_0), \tag{19}$$

if the trajectory touches the classical boundary at time t_0. Without this symmetry the classical trajectory will trace out a new path, as is illustrated in Fig. 7.

The breaking of the time-reversal symmetry can be traced to the paramagnetic term in the Hamiltonian. Examination of the equations of motion and the Hamiltonian reveal that the difficulty lies in the fact that these terms mix odd powers of the momenta and coordinates. The equations of motion can be transformed into a form which is symmetric with respect to time reversal by the simple expedient of switching the identity of the momentum and coordinate of one of the pairs of conjugate variables. This is accomplished in a rigorous manner through the canonical transformation [57] given by

$$v=P_w,$$
$$P_v=-w. \tag{20}$$

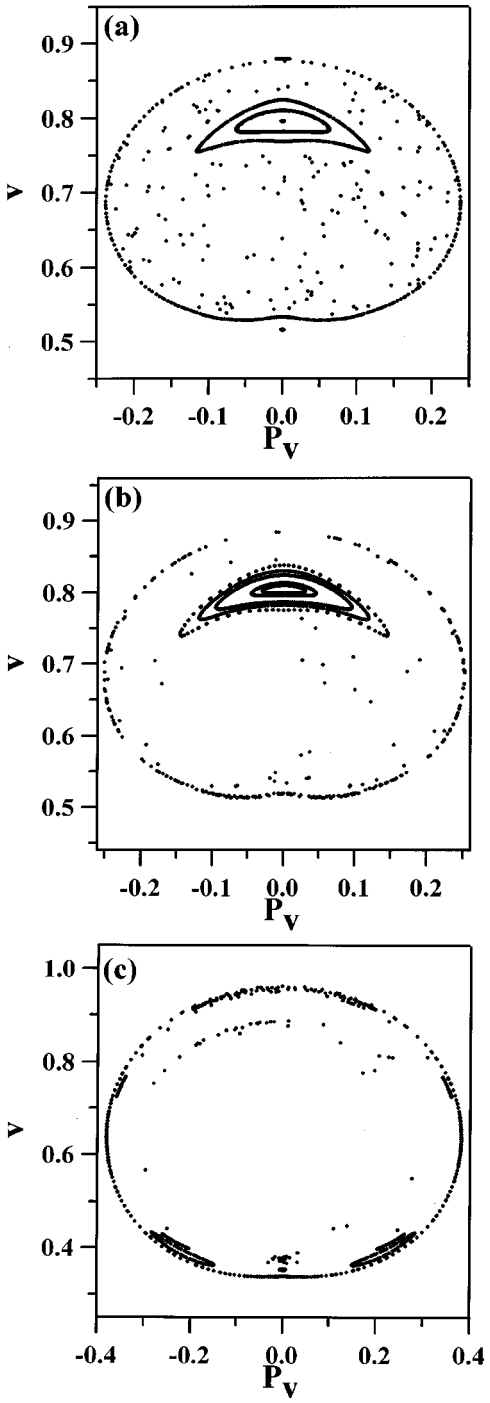

FIG. 5. Shown here are enlargements of the chaotic region in the $(v\text{-}P_v)$ surface of section $(u=0,\dot{u}\geq 0)$ for three values of the electric-field strength (a) $\varepsilon=0.5785$, (b) $\varepsilon=0.58$, and (c) $\varepsilon=0.6$. Observe that at these values of the electric field the chaotic trajectories ionize; in other words, the chaotic sea is drained via ionization. Also note that the central periodic orbit remains stable and is surrounded by *KAM* curves in (a) and (b). For a field strength of $\varepsilon=0.6$ this orbit has become unstable, and the central island of stability has disappeared. However, evidence of higher-order island chains of stability are observed. The axes are the scaled coordinate and the momentum.

Following this well-known transformation [58], the new equations of motion become symmetric with respect to time reversal.

While this transformation solves the central problem of time reversibility, the question of the initial conditions remains. Recall that we wish to start trajectories on the classical boundary. Thus the problem becomes one of identifying the classical boundary in the new coordinate space. In this set of coordinates we can define neither a potential energy nor a zero velocity surface [55], explained at the beginning of Sec. II, and therefore we must seek a new approach. Ob-

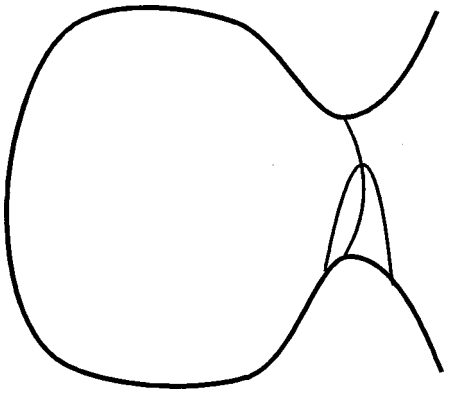

FIG. 6. Shown here is a cartoon illustrating two periodic orbits. The first orbit touches both branches of the equipotential. Orbits of this nature can be used to define transition states. The basic idea is that any trajectory that crosses this orbit from the bound region into the unbound region (that is, from the left to the right) will never return to the bound region. Thus the ionization rate can be obtained by calculating the flux across this orbit. Orbits of this nature can be found by a simple one-parameter search for periodic orbits among the orbits that initially start on an equipotential. Two types of periodic orbits are found in this manner. The first type are orbits that touch both branches of the equipotential, and the second type are orbits that touch the same equipotential twice. The transition state corresponds to an orbit of the first type. This discussion applies to systems which possess time-reversal symmetry. The system under consideration does not possess time-reversal symmetry due to the magnetic field, and thus these ideas must be modified.

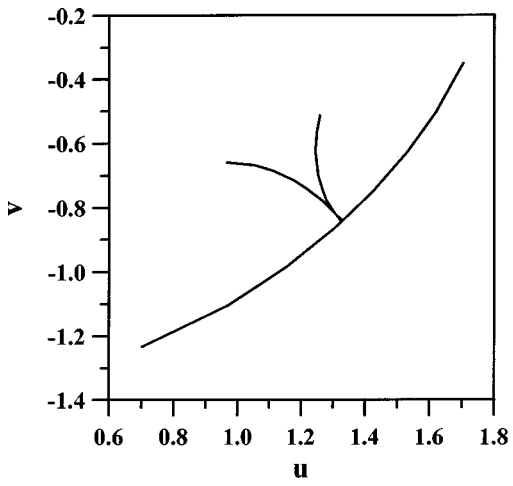

FIG. 7. Shown here is a cartoon that illustrates a difficulty that occurs in systems that do not possess time-reversal symmetry. If a system does possess time-reversal symmetry, then after a trajectory touches an equipotential it will retrace its path in coordinate space. However, in a system that does not possess time-reversal symmetry, an orbit that touches the equipotential will not retrace its path in coordinate space. The observed behavior is illustrated in this figure.

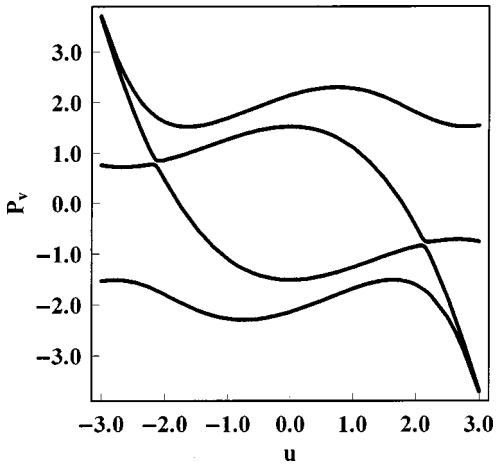

FIG. 8. Shown here are the time-reversal symmetry lines for the hydrogen atom in crossed electric and magnetic fields for an electric-field strength of $\varepsilon = 0.5785$. These lines occur in the (u, P_v) space. The two central curves are the time-reversal symmetry lines of interest in the present problem. Orbits which touch these lines retrace their path in the (u, P_v) space. The periodic orbits that correspond to transition states will touch each of these two branches once. The axes are the scaled coordinate and the momentum.

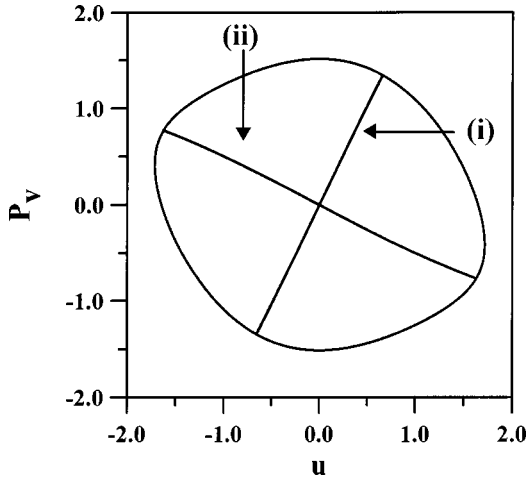

FIG. 9. Shown here are the two periodic orbits (PODS) that touch both time-reversal symmetry lines at an electric-field strength $\varepsilon = 0.4$ well below the onset of chaotic behavior. These two orbits are the central periodic orbits of the nested sets of *KAM* curves observed in Fig. 1 and that are shown in Fig. 2. The axes are the scaled coordinates.

serving that the equipotential and the zero velocity surface contours are time-reversal symmetry lines suggests that one consider these time-reversal symmetry lines in the present case. A time-reversal symmetry line is the solution of $\dot{u} = 0$, and $\dot{P}_v = \dot{w} = 0$ subject to the energy condition $2/\Omega = K(P_u, -w, u, P_w)$. In the present problem four solutions exist to this equation, and are shown in Fig. 8 for $\varepsilon = 0.6$. The upper and lower curves bound the dynamics from above and below, respectively. The two central curves are the solutions of interest to us.

With the equations of motion in a form that is symmetric with respect to time-reversal and with the classical boundaries identified, one is in a position to implement the program discussed above. The time-reversal symmetry line has two branches. These two branches are transformed into each other by inversion, that is, $u \rightarrow -u$ and $P_v \rightarrow -P_v$; thus we need only consider one of these curves. Note that in the (u, v) space this set of initial conditions corresponds to points along the u axis with momentum perpendicular to this axis; that is, $v = 0$ and $P_u = 0$. For one of the branches of the time-reversal symmetry line the momentum P_u is in the positive direction, and on the other it is in the negative direction [see Eq. (17)]. If a given trajectory with these initial conditions intersects the u axis in (u, v) space perpendicularly a second time, then it has touched the other branch of the time-reversal symmetry line. In other words, a segment of the periodic orbit which starts at one of the classical boundaries and ends at the other in (u, P_v) space corresponds to a curve in (u, v) space that starts on the u axis, leaving it perpendicularly, and returning to the u-axis, approaching it perpendicularly. Implementing such a search routine is straightforward.

At field strengths ($\varepsilon = 0.4$) below the ionization threshold two PODS are found, both of which are stable. The projection of these PODS into (u, P_v) space is shown in Fig. 9. Their projection into (u, v) space and (x, y) space were shown in Fig. 2. These are the two fundamental period-1 periodic orbits which the large-scale integrable structures, that is, invariant tori, surround. They persist throughout the range of ε investigated in the present work. Also shown in these figures are the classical boundaries. At field strengths above the ionization threshold ($\varepsilon > 0.5776$), two additional PODS appeared in the vicinity of the two Stark saddles. These PODS ($\varepsilon = 0.6$) are shown in Fig. 10. Note that in

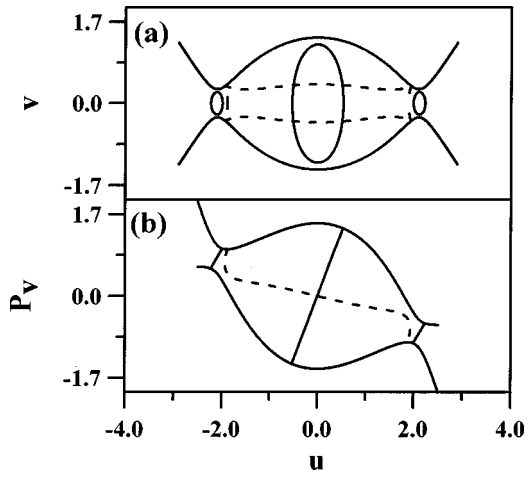

FIG. 10. Shown here are the periodic orbits (PODS) that touch both time-reversal symmetry lines at a field strength $\varepsilon = 0.6$ well above the ionization threshold. The projections of these orbits into the (u, v) space are shown in (a). Here it is seen that these orbits do not touch the equipotentials. The projections of these orbits into the (u, P_v) space are shown in (b). Here it is seen that these orbits touch the time-reversal symmetry lines. The dashed orbits corresponds to the periodic orbit that lies in the center of the chaotic sea [labeled (*ii*) in Figs. 2 and 9]. At this field strength this orbit is unstable. The two small circular orbits on the right and left in (a) are the periodic orbits that correspond to the transition states. In (b) it is seen that these two orbits connect the two branches of the time-reversal symmetry line. The axes are the scaled coordinates.

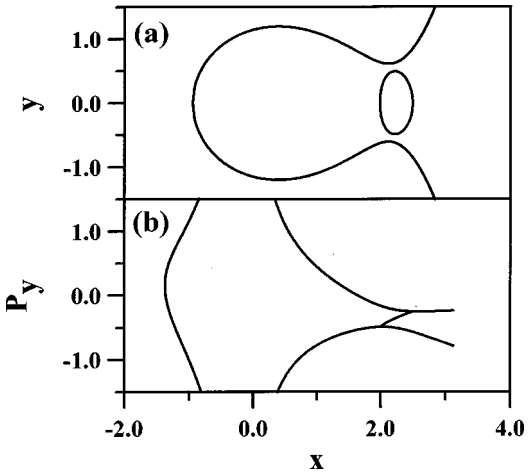

FIG. 11. Shown here is the PODS that corresponds to the transition state. In (a) this orbit is shown in the original Cartesian space (x,y), and in (b) this orbit is shown in the (x,P_y) space. Observe that the PODS does not touch the equipotential in (a) but does touch both branches of the time-reversal symmetry line in (b). The axes are the scaled coordinates.

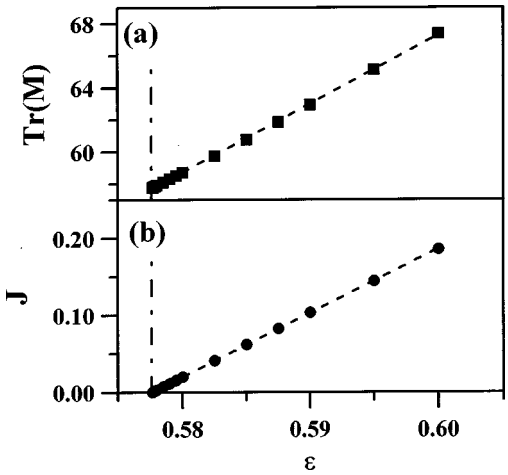

FIG. 13. Shown in (a) is the trace of the stability matrix $\mathrm{Tr}(M)$ and in (b) the classical action J for the transition state PODS as a function of the electric-field strength. Note that the PODS are highly unstable, and that both of these quantities appear to be linear functions of the electric-field strength. The flux across the transition state is proportional to the classical action J.

transforming back into the physical (x,y) space the two PODS in the Stark saddle map into the same orbit; see Fig. 11. This orbit is the transition state: This is evident when one views the projection into either the (u,P_v) space [Fig. 10(b)] or the (x,P_y) space [Fig. 11(b)]. In Fig. 12 we show the transition-state PODS for five different values of the field strength. The trace of the stability matrix M and the classical action J of the transition-state PODS are shown as a function of the field strength in Fig. 13. It should be noted that the PODS is highly unstable and that both J and $\mathrm{Tr}(M)$ appear to be a linear function of the field strength ε.

IV. PHASE-SPACE STRUCTURE

Once the transition state has been identified and found, the investigation of the structure of the volume of phase space that ionizes becomes possible. The central goal is to use the dynamics to partition phase space. This is achieved by construction of the stable manifolds of the PODS associated with the two transition states. Consider the stable manifold of the PODS on the right-hand side; see Fig. 10. This is a two-dimensional surface (tube) within the three-dimensional energy shell that partitions the energy shell. The trajectories that lie within this volume all ionize to the right. In a similar manner all of the trajectories that lie within the stable manifold associated with the PODS on the left-hand side, will ionize to the left. The trajectories that lie outside of both of these stable manifold will never ionize; that is, they are bound. In order to examine the time development of the system we construct a surface of section that intersects this partitioning transversely, that is, we chose our surface of section plane in such a manner that one of the stable manifolds intersects it once each period. As will be explained below this yields a fractal tiling [59] of the surface of section. It is this partitioning of the surface of section that is needed in order to discuss the half-scattering problem. For example, the scaling laws of this fractal determine the classical rate of ionization.

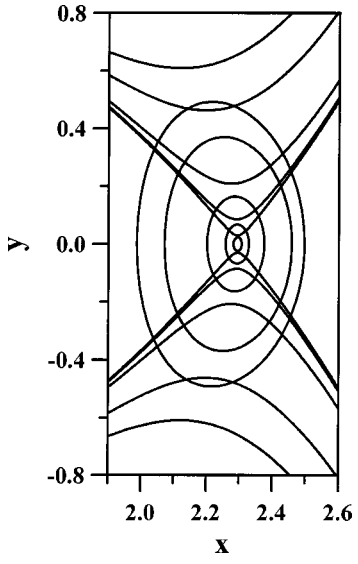

FIG. 12. The five transition-state PODS for different values of the electric-field strength are shown in this figure. These are shown in the original Cartesian space (x,y). The axes are the scaled coordinates.

A similar partitioning of the energy shell can be constructed using the unstable manifolds. By combining these two partitionings of the energy shell, one obtains an invariant fractal tiling of the energy shell. It is this partitioning of the energy shell that is needed to discuss the full scattering problem. For example, the scaling laws of this partitioning will determine the average lifetime of atomic states that are formed in a collision.

In the following we will characterize these partitionings and investigate how they change as a function of the strength of the electric field. At the heart of the method are (i) the correct choice of the surface of section and (b) the constructions of the manifolds in phase space. We now turn to these two critical issues.

A. Choice of the surface of section

While the choice of surface of section is of little consequence mathematically, it can have a significant impact on

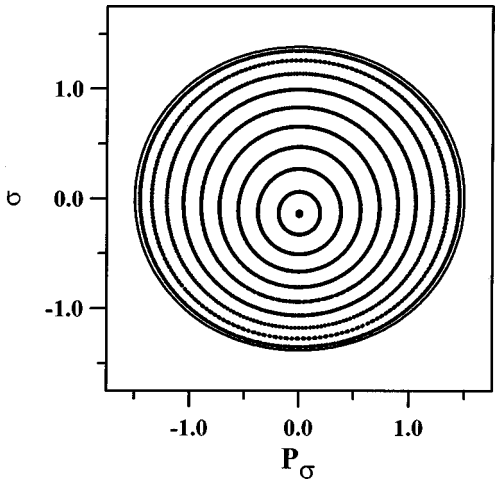

FIG. 14. Shown here is a periodic orbit surface of section for an electric-field strength of $\varepsilon = 0.4$ constructed using the periodic orbit labeled (*i*) in Figs. 2 and 9. This surface of section should be compared with the surface of section shown in Fig. 1. Both are constructed from the same data. The use of a periodic orbit to construct this surface of section avoids the difficulties observed in Fig. 1, and makes clear that at this field strength the dynamics are analogous to those of two weakly coupled oscillators. The axes are the scaled coordinate and the momentum.

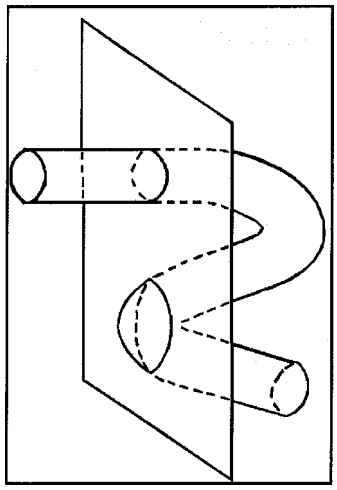

FIG. 15. Shown in this figure is a schematic illustrating the difficulties that can arise if one does not use a periodic orbit to define ones surface of section. Consider the dynamics that are confined to the tube shown here. The plane is the surface of section. Clearly one can obtain closed circular figures in the surface of section in two different manners. If the tube intersects the plane one will obtain a closed circle, but also note that one can obtain a circular figure if only an elbow of the tube intersects the surface of section plane. Poincaré was aware of difficulties of this nature. They will occur whenever a classical trajectory touches the surface of section plane tangentially. These difficulties can be avoided by defining ones surface of section using a classical trajectory.

the ease of interpretation. In order to ensure easy interpretation, it is best to choose a surface of section along one of the central periodic orbits (see Fig. 2). There are two reasons for this: First, with this choice the classical boundary of the surface of section will correspond to the periodic orbit; and second, we ensure that no trajectories intersect the surface of section tangentially in the range of electric field strengths of interest. The first of these difficulties is seen in the surfaces of section shown in Sec. II. Here we see two sets of foliated *KAM* curves even though no separatrix exists to separate them. If we construct the surface of section using the central periodic orbit of the lower pattern [labeled (*i*) in Fig. 2], then in place of Fig. 1 we obtain Fig. 14. This periodic orbit is the classical boundary of the surface of section shown in Fig. 14. The central periodic orbit of the upper set of foliated *KAM* curves in Fig. 1 [labeled (*ii*) in Fig. 2] is the central periodic orbit in the new surface of section. The new surface of section, which we will call the ''periodic orbit surface of section,'' for this system is simply what one expects for two coupled oscillators.

Figure 15 shows an example of what can happen if one constructs a surface of section using a curve that is not a trajectory. The plane shown is the phase-space surface that is used to construct the surface of section. The tube is an invariant phase-space surface constructed from trajectories. If one of the trajectories used to construct the tube intersects the surface of section plane tangentially, then one will obtain extraneous closed figures in the surface of section. These figures are artifacts of the choice of the surface of section. It is interesting that these difficulties were known to Poincaré [60]. Generally, the use of a periodic orbit to construct the surface of section avoids problems of this nature. While this choice of surface of section does increase the complexity of the calculations, it prevents errors and leads to a clearer exposition. The technical details of the construction of this surface of section are provided in the Appendix.

B. Construction of the manifolds

The PODS associated with the transition states are unstable periodic orbits. As a consequence, they possess stable and unstable manifolds which may be constructed as follows: Initial conditions for the PODS are obtained on a convenient surface of section. In this case we used the (u, P_u) surface of section ($v = 0, \dot{v} \gtrless 0$). The stability matrix is constructed using four slightly perturbed trajectories. The eigenvectors of this matrix define the stable and unstable directions in the surface of section. An initial condition is then chosen very close to the PODS with the perturbation from the PODS being chosen in the unstable direction. The trajectory is then followed forward in time until it intersects the surface of section again. If this second intersection is still within the linear region of the PODS—that is, the PODS, the initial condition, and its first image all lie on a straight line—then a set of initial conditions are constructed on a grid on the line segment connecting the initial condition and the first intersection. Integrating these initial conditions forward in time yields the unstable manifold. The corresponding stable manifold is obtained using the time-reversal symmetry of the system. In turn, the manifolds of the other PODS are obtained by a simple inversion.

C. Ionization

In order to investigate the dynamics of ionization we construct the periodic orbit surface of section of the stable manifolds for the two PODS associated with the transition states; see Fig. 10. All of the states that ionize are confined within

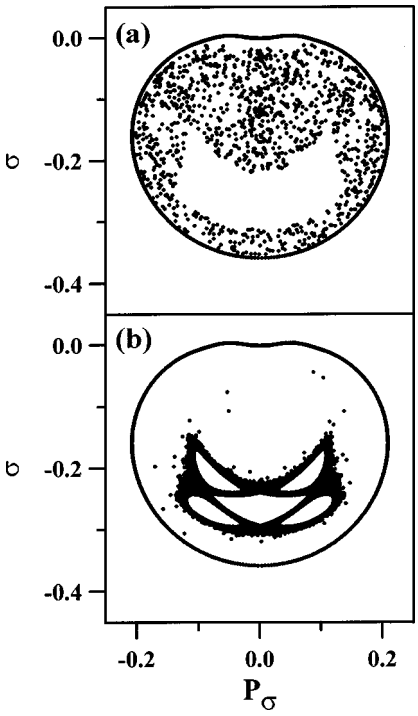

FIG. 16. The periodic orbit surface of section for two chaotic trajectories for an electric-field strength $\varepsilon = 0.57765$ just above the ionization threshold are shown in this figure. The orbit shown in (a) survives 2384 periods before ionization, while that shown in (b) survives 77 613 periods. Finding long-lived trajectories of this nature is not difficult at this value of the electric-field strength. By observing these trajectories develop it is clear that they are trapped behind a series of bottlenecks. The axes are the scaled coordinate and the momentum.

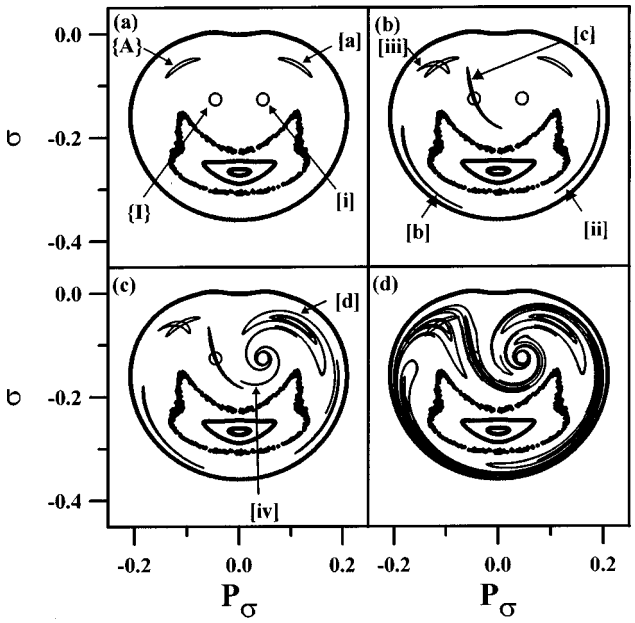

FIG. 17. Shown here are the stable manifolds of the two PODS in the periodic orbit surface of section for an electric-field strength $\varepsilon = 0.57765$. Shown in (a) are the two sinks labeled $[i]$ and $[a]$ and the two sources labeled $\{I\}$ and $\{A\}$. Shown in (b), in addition to the sinks and sources, are the first ($[ii]$, $[b]$) and second ($[iii]$, $[c]$) preimages of the two sinks. Shown in (c), in addition to the sinks, sources, and their first and second preimages, are the third preimages $[iv]$ and $[d]$ of the two sinks. Finally, in (d), the sinks and sources and the first five preimages of the sinks are shown. Of particular interest is the manner in which the preimages swirl around the sinks and intersect the sources. The axes are the scaled coordinate and the momentum.

these two manifolds. The stable manifolds are two-dimensional tubes within the three-dimensional energy shell. Consequently, each time one of the manifolds crosses the surface of section, a closed curve is generated. However, these closed curves do not intersect. Further, the areas enclosed within these curves, taken together with the bound states, cover the entire surface of section. In other words, they form a tiling [59] of the surface of section. Each of the enclosed areas is called a ''tile,'' as will explained in the following discussion.

We begin by considering the ionization dynamics just above the ionization threshold, $\varepsilon = 0.57765$. The chaotic region of the surface of section is shown in Fig. 16. The continuous outer curve is an invariant torus that bounds the chaotic region. In Fig. 16(a) the scattered points correspond to a single trajectory that survives for 2384 periods [61]. Finding trajectories that survive this long is not difficult at this value of ε. Out of 15 trajectories examined in the chaotic region (chosen on a uniform grid on the symmetry line of the surface of section, $P_y = 0$), one corresponded to an island of stability, and three survived for more than 2000 periods. It is much more difficult to find trajectories that correspond to short lifetimes; out of these 15 trajectories, only one survived for fewer than 50 periods. In Fig. 16(b) we show a truly exceptional long-lived trajectory; it is trapped behind a series bottlenecks and survives for a whopping 77 613 periods. This is clearly a case of ''delayed'' ionization [68].

Consider the last intersection of the stable manifold of the PODS on the left with the surface of section. This tile is labeled $[i]$ in Fig. 17(a), all trajectories that pass through this tile ionize immediately to the left. Now consider the last intersection of the stable manifold of the PODS on the right. This tile is labeled $[a]$ in Fig. 17(a); all trajectories that pass through this tile ionize to the right after an additional period. These two tiles are the sinks in the surface of section. It is important to recognize that the existence of two sinks is a result of the doubling of the phase space due to the regularization of the Hamiltonian discussed in Sec. II. If one transforms back to their physical (nonregularized) variables, these two sinks would be mapped into a single sink. Now follow the states represented by these two tiles backward in time until they once again intersect the surface of section. We refer to these intersections as the preimages of the tiles (sinks). The preimages of the sinks are shown in Fig. 17(b), and are labeled $[ii]$ and $[b]$, respectively. Also shown in this figure are the preimages of $[ii]$ and $[b]$; they are labeled $[iii]$ and $[c]$, respectively. A trajectory that passes through tile $[iii]$, will pass next through tile $[ii]$, and then through tile $[i]$ to ionize to the left. The flux through these tiles is equal to their areas. Further, the area of each of the tiles seen in this figure is equal to the flux across the transition state. The same holds for the tiles associated with ionization to the left; that is, $[c] \rightarrow [b] \rightarrow [a]$.

Also shown in Fig. 17 are the first intersections of the unstable manifolds of the two PODS associated with the

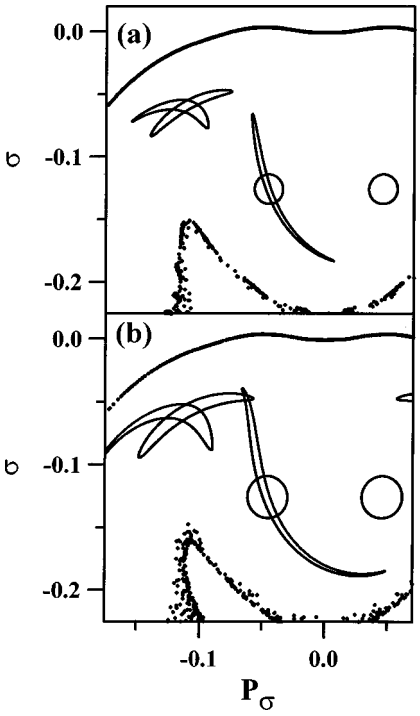

FIG. 18. Shown here are enlargements of the periodic orbit surface of section in the region of the two sources, $\{I\}$ and $\{A\}$ for electric-field strengths of $\varepsilon = 0.577\,65$ for (a) and $\varepsilon = 0.5777$ for (b). Of particular interest here are the intersections of the tiles $[iii]$ and $[c]$. The areas interior to these tiles will ionize in three periods. The areas interior to the intersections of these tiles with the sources are captured in the previous period, and thus will only be bound for four periods. The axes are the scaled coordinate and the momentum.

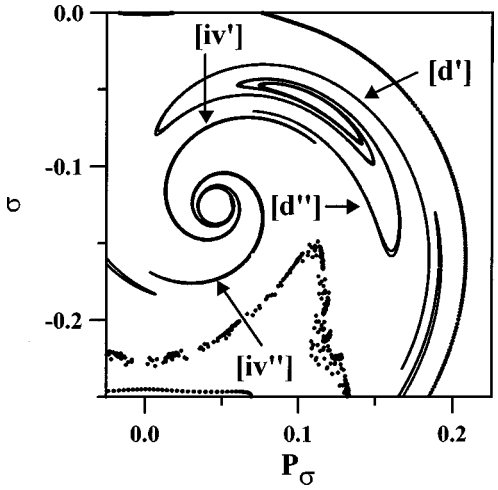

FIG. 19. Shown here is an enlargement of the periodic orbit surface of section in the region of the two sinks $[i]$ and $[a]$ for an electric-field strength of $\varepsilon = 0.57765$. Seen here are the third preimages of the two sinks $[iv]$ and $[d]$ which are swirling around the sinks. These tiles have bifurcated. The axes are the scaled coordinate and the momentum.

transition states. These are labeled $\{I\}$ and $\{A\}$ and are associated with capture of an electron from the right and the left, respectively. We label these areas with curly brackets to indicate that they are sources. Observe in Fig. 17(b) that tile $[iii]$ intersects the area $\{A\}$ and $[c]$ intersects the area $\{I\}$. An enlargement of these intersections is shown in Fig. 18(a). The area interior to both $[iii]$ and $\{A\}$ corresponds to trajectories that were captured in the previous period from the right, and which will ionize to the left in four periods. The part of the tile $[iii]$ that is interior to $\{A\}$ does not have a preimage. As a consequence, the preimage of $[iii]$ will be partitioned into two tiles, which are shown and labeled $[iv']$ and $[iv'']$ in Fig. 19. Observe that the tiles $[iv']$ and $[iv'']$ swirl infinitely often around $[i]$. Note that the flux through these tiles is equal to the combined areas of the tiles. Similar arguments hold for the intersection of $[c]$ and $\{I\}$. Here the area of tile $[c]$ interior to $\{I\}$ correspond to trajectories that have just been captured from the right and will ionize to the left in five periods. The preimage of $[c]$ consists of the two tiles $[d']$ and $[d'']$ (see Fig. 19). A composite of all these features is shown in Fig. 17(c).

The preimages of tiles $[iv']$ and $[iv'']$, that is $[v']$ and $[v'']$, swirl infinitely often around $[ii]$ and then the preimages of $[v']$ and $[v'']$; that is, $[vi']$ and $[vi'']$, swirl infinitely often around $[iii]$. As a consequence of tiles $[vi']$ and $[vi'']$ swirling infinitely often around $[iii]$, they will intersect the area $\{A\}$ infinitely often. This is shown in Fig. 20. Thus, the preimage of each of the tiles $[vi']$ and $[vi'']$ will consist of two infinite sets of tiles. These tiles, which we do not attempt to show, are wrapped around the tiles $[iv']$ and $[iv'']$ which in turn are wrapped around $[i]$. This process continues *ad infinitum*, yielding structure on all scales. We are forced to conclude that this tiling is fractal. A composite surface of section for the tiles $[i] \rightarrow [vi]$ and $[a] \rightarrow [f]$ is shown in Fig. 17(d). The stretching and swirling of the phase-space dynamics is clear.

The dynamics associated with each of the tiles can be characterized by two integers (n,m). The first of these, n, indicates the number of periods required for the trajectory to be ionized, that is, to cross the transition state. This is related to the number of times that the trajectory crosses the periodic orbit defining the surface of section. The second integer m

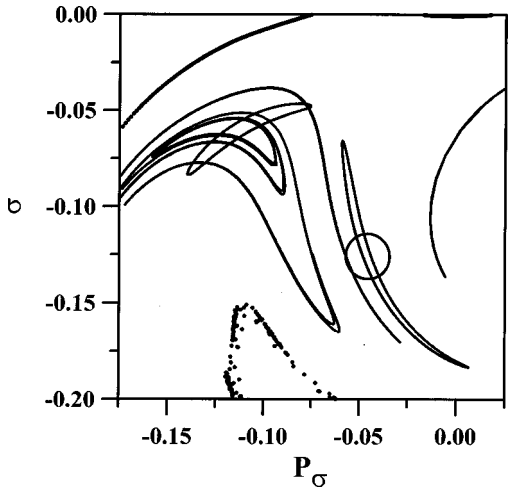

FIG. 20. Shown here is an enlargement of the periodic orbit surface of section in the region of the two sources, $\{I\}$ and $\{A\}$, for an electric-field strength of $\varepsilon = 0.57765$. Seen here are the tiles $[v']$ and $[v'']$, which are swirling around the tile $[ii]$, and tiles $[vi']$ and $[vi'']$, which are swirling around tile $[iii]$. As consequence, these tiles intersect the source infinitely often. The axes are the scaled coordinate and the momentum.

indicates the number of times the trajectory crosses the periodic orbit transverse to the orbit defining the surface of section. The sets of infinite sequences of tiles mentioned above, resulting from the infinite swirling, correspond to dynamics characterized by a given n and different m's.

The dynamics of ionization are more complicated than is illustrated in the example just presented. In this example, the electrons were captured from the right and ionized to the right or were captured from the left and ionized to the left. In other words, during the lifetime of the atomic state (that is, from formation until ionization) the electrons orbit the nucleus an odd number of times. Classical trajectories corresponding to atomic states that are characterized by an even number of periods of the electron about the nucleus will be captured from the right and ionized to the left, or vice versa. The reason that this behavior was not observed is not that it does not occur, but rather that we did not investigate the dynamics on a fine enough scale. We consider next the dynamics for a value of the electric-field strength where behavior of this nature is more readily observed. Tile $[c]$ for $\varepsilon = 0.5777$ is shown in Fig. 18(b). This tile intersects both areas $\{I\}$ and $\{A\}$. The atomic states associated with the area enclosed in the intersection of $[c]$ and $\{I\}$ corresponds to atomic states that survive for five periods. The atomic states within this intersection are both captured from and ionized to the right. On the other hand, the atomic states associated with the area enclosed in the intersection of $[c]$ and $\{A\}$ survive six periods and are captured from the right and ionized to the left. As a consequence of tile $[c]$ intersecting both areas $\{I\}$ and $\{A\}$, the preimage of $[c]$ will consist of three tiles $[d']$, $[d'']$, and $[d''']$. These tiles are shown in Fig. 21. Tile $[d']$ swirls around $[a]$ [Fig. 21(a)], $[d''']$ swirls around $[i]$ [Fig. 21(c)], and $[d'']$ swirl around both $[i]$ and $[a]$ [Fig. 21(b)]. The preimages of these three tiles, which we would label $[f']$, $[f'']$, and $[f''']$, will swirl around tiles $[a]$ and $[ii]$. Clearly, with a bit of care, one can follow these dynamics and unravel the complexity; however, these details are not required to make further progress in understanding the features of the dynamics that determine the ionization rates.

This example elucidates how the fractal tiling evolves as the field strength ε is increased [compare Figs. 18(a) and 18(b)]. This is illustrated in Fig. 22, where sinks $[i]$ and $[a]$ and sources $\{I\}$ and $\{A\}$ are shown for three values of ε ($\varepsilon = 0.578$, 0.5783, and 0.5785). This range of values of the field strength corresponds to intermediate lifetimes (10–100 periods). In Fig. 22(a) ($\varepsilon = 0.578$) one sees that tile $[a]$ intersects with area $\{A\}$. The portion of tile $[a]$ that is enclosed within area $\{A\}$ corresponds to trajectories that have been captured from the left in the previous period and will ionize to the right in the next period, and thus survive for two periods. The result of increasing the field strength a small amount is seen in Fig. 22(b) ($\varepsilon = 0.5783$). Here we see that now tile $[a]$ intersects area $\{I\}$ and that tile $[i]$ intersects area $\{A\}$. The intersecting areas here correspond to atomic states that survive for a single period. This corresponds to the onset of ''prompt'' ionization [68]. Finally in Fig. 22(c) we see that at $\varepsilon = 0.5785$ tile $[i]$ intersects area $\{I\}$. The area enclosed in this intersection corresponds to direct collisions. In other words, the electron approaches from the right and immediately leaves (without orbiting the nucleus) to the left. The onset of direct scattering occurs between $\varepsilon = 0.5783$ and $\varepsilon = 0.5784$. It should be noted that a direct scattering trajectory that approaches from the left and leaves to the right never crosses the surface of section. It should also be observed that the onset of direct scattering coincides with the tile $[a]$ swirling infinitely often around tile $[i]$. Similarly, area $\{A\}$ swirls infinitely often around area $\{I\}$.

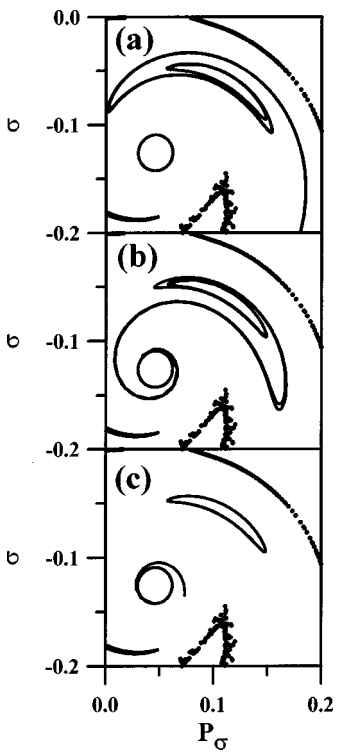

FIG. 21. Shown here is an enlargement of the periodic orbit surface of section in the region of the two sinks $[i]$ and $[a]$ for an electric-field strength of $\varepsilon = 0.577\,70$. Seen here is the third preimage of tile $[a]$. This preimage has bifurcated into three tiles $[d']$, $[d'']$, and $[d''']$. The tile $[d']$ swirls around $[a]$ [seen in (c)], and tile $[d'']$ swirls around both tiles $[a]$ and $[i]$ [seen in (b)] and tile $[d''']$ swirls around $[i]$ [seen in (a)]. The axis are the scaled coordinate and momentum.

The structure of phase space continues to evolve as the field strength is increased. This is illustrated in Fig. 23, where the first five tiles are shown for $\varepsilon = 0.58$, 0.59, and 0.6. In this range of field strengths the lifetimes are short (0–10 periods). A number of features should be noted: First, observe the island of stability. This island shrinks rapidly; between $\varepsilon = 0.595$ and 0.6 the central periodic orbit becomes unstable and the island disappears. The unstable periodic orbit is shown as a dashed curve in Fig. 10. Also observe that the area of the chaotic region increases as does the area of the tile $[i]$; however, the area of the tile increases more rapidly than the area of the chaotic region, which in turn squeezes the other structure at the expense of the higher-order tiles. We also observed that in the vicinity of the outer boundary there exist many small islands of stability: associated with these are bottlenecks analogous to those observed just above the ionization threshold. Consequently, here again we can find trajectories with lifetimes that are extremely long.

Another way of investigating the fractal structure is to construct the underlying Cantor set. This can be accomplished in a manner analogous to the construction of the $\frac{1}{3}$

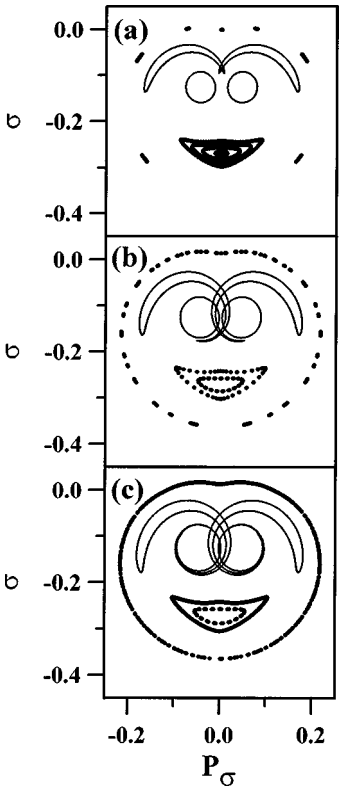

FIG. 22. Shown here is the scattering region of the periodic orbit surface of section for three different values of the electric-field strength: (a) $\varepsilon = 0.578$, (b) $\varepsilon = 0.5783$, and (c) $\varepsilon = 0.5785$. In these figures we show the development of the sources and sinks as the electric field is increased. In (a) we see the first intersection of a sink $[a]$ and a source $\{A\}$. This corresponds to the onset of direct ionization. As the electric field is increased the sink $[a]$ intersects with both sources $\{A\}$ and $\{I\}$. As the electric field is increased further the sink $[i]$ intersects with the sources $\{I\}$. The axes are the scaled coordinate and the momentum.

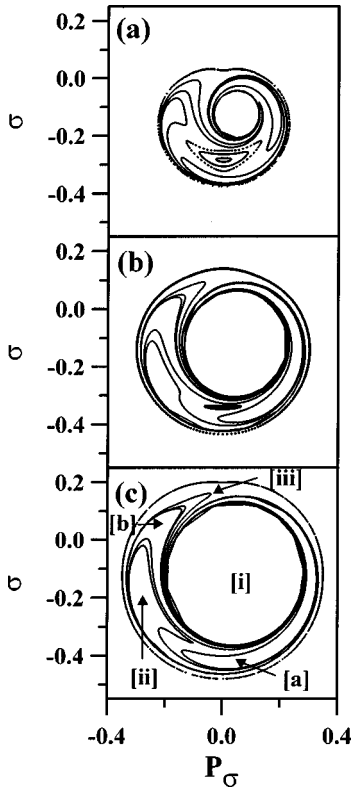

FIG. 23. Shown here is the development of the tiling of the periodic orbit surface of section as the electric-field strength is increased: (a) $\varepsilon = 0.58$, (b) $\varepsilon = 0.59$, and (c) $\varepsilon = 0.60$. The axes are the scaled coordinate and the momentum.

Cantor set [62]: Start with the first intersection of the unstable manifold associated with the PODS on the right, that is, the boundary of area $\{I\}$. When the first tile intersects this curve (see Fig. 18), remove the portion of the curve that is interior to the tile. Repeat this procedure for the second tile that intersects the curve, and then again for the third and subsequent tiles. In the infinite limit we will have removed the entire length of the curve, yet there will remain a set of points of measure zero. The set of trajectories associated with this set of points is the Cantor set underlying the dynamics. Included in this set of points are the intersection points of the original curve and the boundaries of the tiles. These intersection points are associated with the doubly asymptotic trajectories, that is, homoclinic and heteroclinic orbits. Also included in this set of trajectories are the unstable periodic orbits that exist above the ionization threshold.

D. Scaling laws of the fractal tiling and the classical rate of ionization

A necessary question in any discussion of a fractal occurring in a physical system is the relationship between the properties of the fractal and the physical observables of the system. In the present case there is a direct relation between the ionization rate and the scaling laws of the fractal: each tile is characterized by the number of periods that is required for the states within the tile to ionize. We will refer to the tiles that require n periods to ionize as tiles of the nth generation [52]. The flux through a tile is proportional to its area. If we call the sum of the areas of tiles of the nth generation α_n, then we expect that these areas will scale in the limit $n \to \infty$ as

$$\alpha_{n+1} = \eta \alpha_n . \tag{21}$$

If this is the case, then, in the long-time limit, we expect the number of states ionizing during each period to be an exponential function of the number of periods, that is,

$$F_n \propto e^{-nk} = \eta^n, \tag{22}$$

where the rate constant is given by $k = -\ln \eta$. The survival probability (that is, the number of states that have not ionized after n periods) is given by

$$S_n = 1 - \sum_m F_m \propto e^{-nk} = \eta^n. \tag{23}$$

The survival probabilities for several values of the field strength ($\varepsilon = 0.5777$, 0.5785, and 0.6) are shown in Fig. 24. Here we see that following some induction period, the survival probability is exponential verifying our expectations concerning the scaling law [Eq. (21)], which governs the flux through the tiles. Observe that the induction period can be

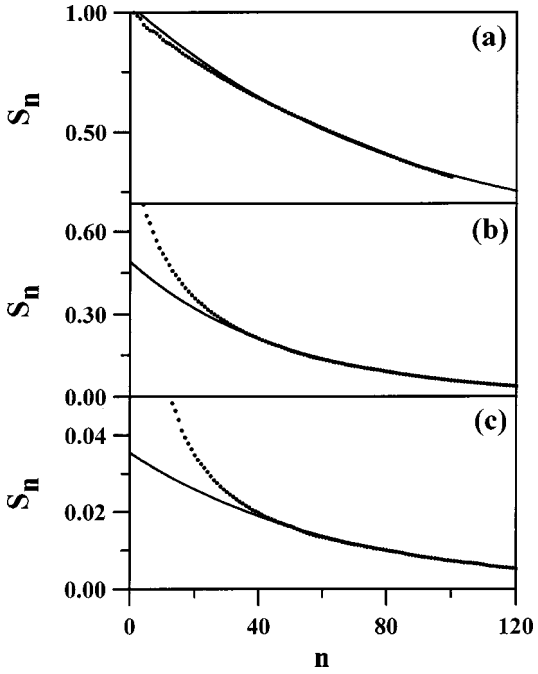

FIG. 24. Shown here are the survival probabilities for three values of the electric-field strength: (a) $\varepsilon = 0.5777$, (b) $\varepsilon = 0.5785$, and (c) $\varepsilon = 0.60$.

relatively long (30 periods in the case of $\varepsilon = 0.5785$). This is the ionization induction period for ''delayed'' ionization [68].

E. Fractal dimensions

Another important property of the fractal tiling of the surface of section that is of interest in characterizing the ionization dynamics is the fractal dimension. This quantity can be interpreted as a measure of the degree of mixing of the dynamics. In determining this quantity we have followed the pioneering work of Grebogi *et al.* [63] on the dimensionality of the boundaries of fractal basins. As we have seen above, in the regularized coordinates, the electron can ionize to either the right or the left. Ionization to the right requires an odd number of periods, while ionization to the left requires an even number of periods. Clearly, every point in the chaotic region of the surface of section can be characterized as ionizing to either the right or the left.

The prescription outlined by Grebogi *et al.* requires that one choose pairs of initial conditions that are separated by a small quantity λ. Trajectories emanating from a pair of initial conditions are then calculated. These trajectories are followed until they ionize. If they ionize in opposite directions then the pair of trajectories is said to be uncertain. This procedure is repeated a large number of times in order to calculate the fraction of trajectories F that are uncertain as a function of the small quantity λ. This fraction is expected to exhibit a power-law dependence

$$F_\varepsilon(\lambda) \propto \lambda^{D-\delta_\varepsilon}, \tag{24}$$

where D is the dimension of the space from which the initial conditions are chosen, and δ_ε is the uncertainty dimension of the boundary between the two basins.

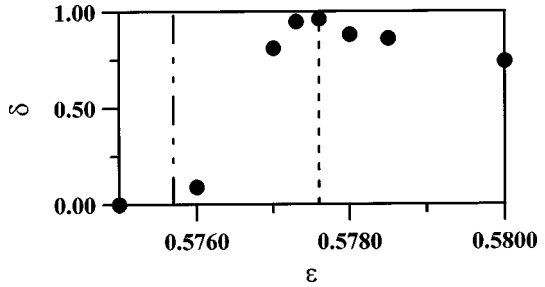

FIG. 25. Shown here is the fractal dimension characterizing the ionization dynamics.

A couple of difficulties arise in the implementation of this procedure. First, recall that for values of the electric-field strength investigated, the lifetimes of the atomic states can be extremely long; consequently, the procedure just outlined requires an excessively long series of calculations. In addition to this, this procedure is only applicable above the ionization threshold. Both these difficulties can be avoided by the following modification of the procedure: Instead of following the pairs of trajectories until they ionize, we follow them for 80 periods (40 intersections with the surface of section), or until they ionize. At this point of time we ask whether the two trajectories on the same side of the symmetry line in the surface of section. If they are not, we say they are ''uncertain.'' Clearly, this modification of the procedure avoids both difficulties mentioned above.

Consider the symmetry line of the (v, P_v) surface of section ($u = 0$, $\dot{u} \geqslant 0$), that is, $P_v = 0$ (see Figs. 1 and 3.). Note that the points on this line correspond to the origin of the (u, P_v) space. Furthermore, it is easy to show that this symmetry line is the time-reversal symmetry line in the (P_u, v) space. In other words, $\dot{P}_u = 0$ and $\dot{v} = 0$. We choose our initial conditions on this symmetry line, and thus, $D = 1$. The results of these calculations are shown in Fig. 25.

The onset of chaos is first observed at $\varepsilon_{\text{crit}} \simeq 0.5757$. Below this value of the field strength the uncertainty dimension δ_ε is equal to zero. In the range $0.5757 < \varepsilon < 0.5776$ the uncertainty dimension increases monotonically, while above the ionization threshold it slowly decreases. This is an interesting result in that it implies that just after the onset of chaos the system is not highly mixing. However, as the field strength is increased, chaos develops and the system becomes more highly mixing. Once the ionization threshold is crossed the degree of mixing decreases which can be attributed to the fact the electron escapes in a finite time and the lifetime of the atomic state limits the degree of mixing.

V. RELATIONSHIP BETWEEN THE HALF- AND FULL-SCATTERING PROBLEMS

The dynamics of the ionization of a planar atom in the crossed electric and magnetic fields is a half-scattering problem. The atom is initially prepared in some highly excited metastable Rydberg state, and we are interested in its behavior in the future. This is very different from the full-scattering problem. In the full-scattering problem the system is prepared in an unbound initial state, and we are interested in the dynamics of formation of a highly excite metastable Rydberg atom and its subsequent ionization. The analysis of

the structure of phase space for these two different types of problems is significantly different.

The central difference between the analysis of the dynamics of the half- and full-scattering problems is that in the half-scattering problem one is only interested in the asymptotic behavior in the infinite future, while in the full-scattering problem one is interested in the asymptotic behavior in both the infinite future and in the infinite past. As a consequence, in the half-scattering problem one need only consider the stable manifolds of the two PODS associated with the transition states as it is these manifolds that determine the dynamical behavior in the infinite future. On the other hand, for the full-scattering problem one must consider both the stable and unstable manifolds of the PODS; the stable manifolds determine the behavior in the infinite future, and the unstable manifolds determine the dynamical behavior in the infinite past.

The stable manifolds partition the energy shell into three parts: one is associated with ionization to the right, another with ionization to the left, and the third with the bound states. The unstable manifolds will also partition the energy shell into three volumes: the first two are associated with capture of the electron from either the right or the left, while the third again corresponds to the bound states. In the half-scattering problem we are interested in how the stable manifold partitions the energy shell, while in the full-scattering problem we are interested in how both the stable and unstable manifold partitions the energy shell. These two partitionings are quite different.

Both partitionings lead to fractal tilings. However, in the half-scattering problem it is not the partitioning of the energy shell that is the fractal tiling, rather it is the partitioning of the surface of section that is a fractal tiling. In the full-scattering case the partitioning of the energy shell is a fractal tiling. Consider Fig. 18(a). Here we see, in the periodic orbit surface of section, two intersections of the stable and unstable manifolds. Consider the areas enclosed in both manifolds. In the half-scattering problem each of these enclosed areas are tiles. In order to construct the tiles in the full-scattering problem one must propagate these areas both forward and backward in time. The volume of the energy shell swept out in this manner is a tile in the full-scattering problem. Clearly, in the full-scattering problem the surface of section will intersect a given tile many times. This is illustrated in Fig. 26. Shown in this figure is the surface of section ($\varepsilon = 0.6$) for the three largest tiles resulting from the analysis of the full-scattering problem. As a consequence of these differences, the fractal properties of the two tilings will be different. In the half-scattering case there will be a single scaling-law-dependent stable manifold, while in the full-scattering case there will be two scaling laws, one dependent on the properties stable manifolds and the other dependent on the properties of the unstable manifolds.

The important feature to recognize is that in the half-scattering problem the fractal tiling is a partitioning of the periodic orbit surface of section, while in the full-scattering problem the fractal tiling is a partitioning of the energy shell. In the full-scattering problem the surface of section should be viewed as being a surface of section of the fractal tiling of the energy shell. It should also be observed that the periodic orbit surface of section that we have used to construct the surface of section of the fractal tiling of the energy shell is not the ''natural'' surface of section to use in the investigation of the full-scattering problem. The ''natural'' surface of section should be constructed using a scattering trajectory. When approached from this point of view each of the stable and unstable manifolds corresponds to an infinite curve in the surface of section. The study of the geometry of the intersections of these curves leads to the usual definition of interaction region, and of the turnstiles governing the flux in and out of the interaction region.

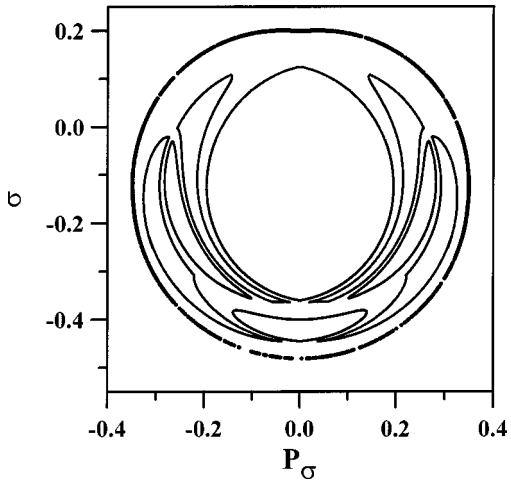

FIG. 26. Shown here are the intersections of the three largest tiles associated with the full-scattering description of the dynamics with the periodic orbit surface of section for an electric-field strength of $\varepsilon = 0.60$. These tiles are distinct from the tiles associated with the half-scattering problem. The axes are the scaled coordinate and the momentum.

VI. CONCLUSIONS

We have shown by construction that there exists a transition state in the planar atom in crossed electric- and magnetic-field problems. This phase-space structure enables us to partition a suitably chosen coordinate space into two regions: The first of these corresponds to bound states, while the second corresponds to ionized states. The fundamental importance of the transition state is that it represents a surface of no return. That is, once the electron crosses the transition state from the bound side to the ionized side, it will never cross back.

We have also shown that the stable manifolds of the PODS associated with the transition state can be used to partition the surface of section into areas that correspond to different ionization lifetimes. These areas form a fractal tiling of the surface of section. We have also demonstrated that the scaling laws of the areas of the tiles are directly responsible for the exponential decay of the ionization probability.

Underlying the fractal structure is an invariant set of trajectories that never escape. Among these trajectories are the periodic orbits of this system. It is these orbits that organize the structure of phase space. The stable periodic orbits are surrounded by invariant tori and are responsible for the islands of stability. The unstable periodic orbits act as attractors and repellers. Their stable and unstable manifolds channel the flow in phase space.

Plainly, a variety of different mechanisms can lead to chaotic behavior, the best known of these being the Smale ''horseshoe'' in which phase space is stretched and folded an infinite number of times [64]. Such structures have been observed in a variety of different systems: The area-preserving Hénon map [65] and the van der Waals molecule HeI_2 [52] are just two examples. The chaotic behavior observed in the present system is not a Smale horseshoe. The chaotic region of the surface of section can be thought of as a bounded region on a cylinder. The structures in phase space are stretched around this cylinder in much the same way as they are stretched in the Smale horseshoe. However, instead of being folded, they are swirled around the two sinks: in one case they are swirled in a clockwise direction and in the other in a counterclockwise direction. After they are swirled, they are stretched around the cylinder again. While this process is quite different from the construction of the Smale horseshoe, the results are quite similar.

ACKNOWLEDGMENTS

This work was supported in part by the National Science Foundation and the Petroleum Research Fund administered by the American Chemical Society. We thank Robin Dallas for her graphical efforts.

APPENDIX: PERIODIC ORBIT SURFACE OF SECTION

In this appendix we discuss the technical details of the construction of the periodic orbit surface of section. Consider Fig. 10. We wish to construct a surface of section using the central periodic orbit shown in this figure. This is accomplished by a series of canonical transformations. The first of these rotates the (u,P_v) coordinate system through an angle θ. We define this angle by drawing a straight line connecting the two points where the classical orbit touches the classical boundaries. θ is the angle that this line makes with the u-axis,

$$\theta=\tan^{-1}\left(\frac{P_v'}{u'}\right),$$

where (u',P_v') are the coordinates of the intersection point. Thus, the new variables are given by

$$r=u\cos\theta-P_v\sin\theta,\quad P_r=P_u\cos\theta-v\sin\theta,$$

$$s=u\sin\theta+P_v\cos\theta,\quad P_s=P_u\sin\theta+v\cos\theta.$$

Next we fit the classical orbit to a cubic spline to obtain $R(s)$, the distance of the classical orbit from the straight line defined above. We now define a new set of coordinates as follows:

$$\rho=r-R(s),\quad P_\rho=P_r,$$

$$\sigma=s,\quad P_\sigma=P_s+P_r\left.\frac{dR(s)}{ds}\right|_{s=\sigma}.$$

In these variables we define the surface of section by ($\rho=0$, $\rho\leqslant 0$), and plot P_σ versus σ. It can happen that s extends beyond the end point of the classical orbit. In order to accommodate this possibility we extend the surface of section plane along the r axis.

Two points are worth remembering: First, we were interested in the crossing of the trajectories from the right to left, and thus we chose $\dot\rho\leqslant 0$ as opposed to the more standard choice of $\dot\rho\geqslant 0$. Second, the common discussion of the difficulties associated with the proper choice of which P_σ branch to use in the construction of the surface of section often results from an improper definition of the surface of section, that is, from defining the surface of section as ($\rho=0$, $P_\rho\leqslant 0$). This is incorrect; see Poincaré [60]. Using the correct definition of the surface of section, one sees that if one simply asks if the classical trajectory has crossed the surface of section plane, that is, if $\rho_{i-1}>0$ and $\rho_i\leqslant 0$, the entire question of which branch it is on becomes moot.

[1] T. Uzer and D. Farrelly, Phys. Rev. A **58**, 4761 (1998).
[2] J. Main and G. Wunner, J. Phys. B **27**, 2835 (1994).
[3] Jean-Patrick Connerade, *Highly Excited Atoms* (Cambridge University Press, Cambridge, England, 1998).
[4] T. F. Gallagher, *Rydberg Atoms* (Cambridge University Press, Cambridge, England, 1994).
[5] G. Herzberg, Annu. Rev. Phys. Chem. **38**, 27 (1987).
[6] R. R. Freeman and D. Kleppner, Phys. Rev. A **14**, 1614 (1976).
[7] P. Bellomo, D. Farrelly, and T. Uzer, J. Phys. Chem. A **101**, 8902 (9197).
[8] B. Eckhardt, Phys. Rep. **163**, 205 (1988).
[9] H. Hasegawa, M. Robnik, and G. Wunner, Prog. Theor. Phys. Suppl. **98**, 198 (1989).
[10] M. Gutzwiller, *Chaos in Classical and Quantum Mechanics* (Springer-Verlag, New York, 1990).
[11] P. M. Koch and K. A. H. van Leeuwen, Phys. Rep. **255**, 289 (1995).
[12] H. Friedrich and D. Wintgen, Phys. Rep. **183**, 37 (1989).
[13] E. A. Solov'ev, Zh. Eksp. Teor. Fiz. **85**, 109 (1983) [Sov. Phys. JETP **58**, 63 (1983)].
[14] P. A. Braun and E. A. Solov'ev, Zh. Eksp. Teor. Fiz. **84**, 68 (1984) [Sov. Phys. JETP **59**, 38 (1984)].
[15] G. Wiebusch, J. Main, K. Krüger, H. Rottke, A, Holle, and K. H. Welge, Phys. Rev. Lett. **62**, 2821 (1989).
[16] G. Raithel, M. Fauth, and H. Walther, Phys. Rev. A **44**, 1898 (1991).
[17] J. von Milczewski, G. H. F. Diercksen, and T. Uzer, Phys. Rev. Lett. **73**, 2428 (1994).
[18] J. von Milczewski and T. Uzer, Phys. Rev. E **55**, 6540 (1997).
[19] D. Delande and J.-C. Gay, in *The Hydrogen Atom*, edited by G. Bassani, M. Inguscio, and T. Haensch (Springer-Verlag, Berlin, 1989), pp. 323 and 334.
[20] A. J. Lichtenberg and M. A. Lieberman, *Regular and Chaotic Dynamics* (Springer-Verlag, New York, 1992).
[21] J. von Milczewski, G. H. F. Diercksen, and T. Uzer, Phys. Rev. Lett. **76**, 2890 (1996).
[22] J. A. Yeazell, G. Raithel, L. Marmet, H. Held, and H. Walther, Phys. Rev. Lett. **70**, 2884 (1993).
[23] J. Main and G. Wunner, Phys. Rev. Lett. **69**, 586 (1992).
[24] T. Uzer and D. Farrelly, Phys. Rev. A **52**, R2501 (1995).

[25] B. R. Johnson, J. D. Hirschfelder, and K. H. Yang, Rev. Mod. Phys. **55**, 109 (1983).
[26] D. Farrelly, Phys. Lett. A **191**, 265 (1994).
[27] M. M. Dignam and J. E. Sipe, Phys. Rev. B **45**, 6819 (1992).
[28] P. Schmelcher, Phys. Rev. B **48**, 14 642 (1993).
[29] A. Bohr and B. R. Mottelson, *Nuclear Structure* (Benjamin Reading, MA, 1975), Vol. II.
[30] G. Mathys, Fundam. Cosm. Phys. **13**, 143 (1989).
[31] F. Mignard, Icarus **49**, 347 (1982).
[32] G. Raithel, M. Fauth, and H. Walther, Phys. Rev. A **47**, 419 (1993).
[33] W. R. S. Garton and F. S. Tomkins, Astrophys. J. **158**, 839 (1969).
[34] G. Raithel and H. Walther, Phys. Rev. A **49**, 1646 (1994).
[35] W. Forst, *Theory of Unimolecular Reactions* (Academic, New York, 1973); P. J. Robinson and K. A. Holbrook, *Unimolecular Reactions* (Wiley, New York, 1992).
[36] M. J. Davis, J. Chem. Phys. **86**, 3978 (1987); M. J. Davis and S. K. Gray, *ibid.* **84**, 5389 (1986).
[37] A. M. Ozorio de Almeida, N. de Leon, M. A. Mehta, and C. C. Marston, Physica D **46**, 265 (1990).
[38] S. Wiggins, *Chaotic Transport in Dynamical Systems* (Springer-Verlag, New York, 1992).
[39] E. Pollak, in *Theory of Chemical Reactions*, edited by M. Baer (CRC Press, Boca Raton, FL, 1985), Chap. 2.
[40] A. Marcelin, Ann. Chim. Phys. **3**, 158 (1915).
[41] H. Eyring and M. Polanyi, Z. Phys. Chem. Abt. B **12**, 279 (1931).
[42] H. Eyring, J. Walter, and G. E. Kimball, *Quantum Chemistry* (Wiley, New York, 1944).
[43] E. P. Wigner, J. Chem. Phys. **5**, 720 (1937).
[44] M. G. Evans and M. Polanyi, Trans. Faraday Soc. **31**, 875 (1935); see also papers and discussion in **34**, (1938).
[45] J. Horiuti, Bull. Chem. Soc. Jpn. **13**, 210 (1937).
[46] G. W. Koeppl, J. Am. Chem. Soc. **96**, 6539 (1974).
[47] J. C. Keck, Adv. Chem. Phys. **13**, 85 (1967).
[48] J. O. Hirschfelder and E. Wigner, J. Chem. Phys. **7**, 616 (1939).
[49] M. J. Davis and E. J. Heller, J. Chem. Phys. **75**, 246 (1980).
[50] P. Pechukas, in *Dynamics of Molecular Collisions*, edited by W. H. Miller (Plenum, New York, 1976), Part B, Chap. 6.
[51] P. Pechukas, Annu. Rev. Phys. Chem. **32**, 159 (1981).
[52] A. Tiyapan and C. Jaffé, J. Chem. Phys. **99**, 2765 (1993); **101**, 10 393 (1994); **103**, 5499 (1995).
[53] E. Flöthmann, Ph.D. thesis, University of Bielefeld, Germany, 1994 (unpublished).
[54] A. Deprit, Astron. J. **71**, 77 (1966).
[55] J. M. Danby, *Fundamentals of Celestial Mechanics*, 2nd ed. (Willman-Bell, Richmond, VA, 1992), pp. 384 and 385.
[56] E. L. Stiefel and G. Scheifele, *Linear and Regular Celestial Mechanics* (Springer-Verlag, Berlin, 1971).
[57] The reason that we choose to exchange the identity of (v,P_v) as opposed to (u,P_u) is that the system ionizes in the u direction, and thus we wish to retain u as one of our dynamical variables.
[58] H. Goldstein, *Classical Mechanics*, 2nd ed. (Addison-Wesley, Reading, MA, 1980), pp. 387 and 388.
[59] B. Grünbaum and G. C. Shepard, *Tilings and Patterns* (Freeman, New York, 1986).
[60] H. Poincaré, *New Methods of Celestial Mechanics*, edited by D. L. Goroff (AIP, New York, 1993), pp. 3, Chap. 27.
[61] Here, and in the following discussion, we refer to periods in the original physical coordinates. Each intersection in the surface of section corresponds to two of these periods. If the electron ionizes to the right it must execute an additional period.
[62] B. B. Mandelbrot, *The Fractal Geometry of Nature* (Freeman, New York, 1983).
[63] C. Grebogi, S. W. McDonald, E. Ott, and J. A. Yorke, Phys. Lett. **99A**, 415 (1983); S. W. McDonald, E. Ott, and J. A. Yorke, Physica D **17**, 125 (1985); S. Bleher, C. Grebogi, E. Ott, and R. Brown, Phys. Rev. A **38**, 930 (1988).
[64] P. Holmes, Phys. Rep. **193**, 137 (1990).
[65] M. Tsuchiya, Ph.D. thesis, West Virginia University, 1996 (unpublished).
[66] U. Fano, in *Atomic Physics 8*, edited by I. Lindgen, A. Rosen, and S. Svanberg (Plenum, New York, 1983), p. 5.
[67] A. R. P. Rau, Rev Mod. Phys. **64**, 623 (1992); T. Pattard and J. M. Rost, Phys. Rev. Lett. **80.** 508 (1998).
[68] A. Muhlpfordt, U. Even, E. Rabani, and R. D. Levine, Phys. Rev. A **51**, 3922 (1995); E. Rabani, R. D. Levin, and U. Even, Ber. Bunsenges. Phys. Chem. **99**, 310 (1995).